Synthesis, X-ray Structure, Electrochemical, and EPR Studies of a Pentacoordinated Mn(II) Tetramethylcyclam Complex

Christophe Bucher,[†] Emmanuelle Duval,[‡] Jean-Michel Barbe,[†] Jean-Noël Verpeaux,[‡] Christian Amatore,*[,‡] Roger Guilard,*[,†] Laurent Le Pape,[§] Jean-Marc Latour,[§] S. Dahaoui,[||] and Claude Lecomte[||]

LIMSAG, UMR 5633, Université de Bourgogne, Faculté des Sciences "Gabriel", 6 Boulevard Gabriel, 21100 Dijon, France, Ecole Normale Supérieure, Département de Chimie (UMR 8640), 24 rue Lhomond, 75231 Paris, Cedex 05, France, Laboratoire DRFMC/Scib/MP (UMR 5046, CEA-CNRS-UJF), CEA-Grenoble, 38054 Grenoble Cedex 9, France, and Laboratoire de Cristallographie et de Modélisation des Matériaux Minéraux et Biologiques (LC3MB), UPRESA 7036, Université Henri Poincaré, Nancy 1, Faculté des Sciences, B.P. 239, 54506 Vandoeuvre lès Nancy Cedex, France

Received December 22, 2000

Introduction

It is well-known that manganese has a fundamental importance in bioinorganic chemistry. Particularly, over the past decade there has been a considerable interest in synthesizing biomimetic complexes that can act as manganoenzymes such as superoxide dismutase (SOD).[1,2] In this field of great interest, linear polyamines and polyazamacrocycles have been extensively studied because of their possible relevance to these biological systems. For example, many complexes based on tri-, tetra-, or pentaazamacrocycles[3−7] as well as porphyrins[8−10] have been shown to exhibit interesting catalytic activities. Among them, several manganese cyclam complexes have been well characterized like a mixed valence Mn(III)−Mn(IV) derivative,[11−13] *C*-substituted Mn(III) derivatives,[14,15] and unsubstituted manganese(III) cyclam derivatives.[16−18] As part of our work on the coordination chemistry of substituted cyclam macrocycles,[19,20] we investigated the complexation of manganese with the 1,4,8,11-tetramethyl-1,4,8,11-tetraazacyclotetradecane (tmc). In accordance with the well-established steric and electronic influences of *N*-substitution,[21−25] and contrary to the case of the unsubstituted homologues, no Mn(III) or dimer mixed valence species could be obtained.

Tetrasubstituted cyclam derivatives are indeed known to stabilize low-oxidation state metal ions and induce steric hindrance, which strongly modifies the complex geometry. As a matter of fact, X-ray structures of cobalt(II)[26] and zinc(II)[27] tmc complexes reported in the literature exhibit similar type I configurations according to Bosnich nomenclature, whereas Ni(II),[28−31] copper(II),[20,32] and iron(II)[33,34] complexes have been found to adopt either a pentacoordinated I, hexacoordinated *trans*-III, or hexacoordinated *trans*-I geometry depending upon the experimental conditions. In our case, the only isolated product is a stable monomeric manganese(II) complex, which results from the reaction of anhydrous manganese(II) salt with the free tmc ligand under argon. Since neither structural nor physicochemical data were reported concerning cyclam-based manganese(II) complexes, we investigated electrochemical, EPR, and variable-temperature magnetism data of [(tmc)MnCl]·X.

* Correspondence should be addressed to Prof. R. Guilard. E-mail: Roger.Guilard@u-bourgogne.fr. Fax: +333 80 39 61 17.
[†] Université de Bourgogne.
[‡] Ecole Normale Supérieure.
[§] Laboratoire DRFMC/Scib/MP.
[||] Université Henri Poincaré.

(1) McCord, J. M.; Fridovich, I. *J. Biol. Chem.* **1969**, *244*, 6049.
(2) Michelson, A. M.; McCord, J. M.; Fridovich, I. *Superoxide and Superoxide Dismutases*; Academic Press: New York, 1977.
(3) Wieghardt, K.; Bossek, U.; Nuber, B.; Weiss, J.; Bonvoisin, J.; Carbella, M.; Vitols, S. E.; Girerd, J. J. *J. Am. Chem. Soc.* **1988**, *110*, 7398.
(4) Hage, R.; Iburg, J. E.; Kerschner, J.; Koek, J. H.; Lempers, E. L. M.; Martens, R. J.; Racherla, U. S.; Russell, S. W.; Swarthoff, T.; Vanvliet, M. R. P.; Warnaar, J. B.; Vanderwolf, L.; Krijnen, B. *Nature* **1994**, *369*, 637.
(5) Riley, D. P.; Weiss, R. H. *J. Am. Chem. Soc.* **1994**, *116*, 387.
(6) Riley, D. P.; Henke, S. L.; Lennon, P. J.; Weiss, R. H.; Neumann, W. L.; Rivers, W. J.; Aston, K. W.; Sample, K. R.; Rahman, H.; Ling, C. S.; Shieh, J. J.; Busch, D. H.; Szulbinski, W. *Inorg. Chem.* **1996**, *35*, 5213.
(7) De Vos, D.; Bein, T. *J. Chem. Soc., Chem. Commun.* **1996**, 917.
(8) Meunier, B.; Guilmet, E.; De Carvalho, M. E.; Poilblanc, R. *J. Am. Chem. Soc.* **1984**, *106*, 6668.
(9) Dismukes, G. C.; Sheats, J. E.; Smegal, J. A. *J. Am. Chem. Soc.* **1987**, *109*, 7202.
(10) Groves, J. T.; Stern, M. K. *J. Am. Chem. Soc.* **1988**, *110*, 8628.
(11) Brewer, K. J.; Liegeois, A.; Otvos, J. W.; Calvin, M.; Spreer, L. O. *J. Chem. Soc., Chem. Commun.* **1988**, 1219.
(12) Brewer, K. J.; Calvin, M.; Lumpkin, R. S.; Otvos, J. W.; Spreer, L. O. *Inorg. Chem.* **1989**, *28*, 4446.
(13) Goodson, P. A.; Hodgson, D. J. *Inorg. Chim. Acta* **1990**, *172*, 49.
(14) Bryan, P. S.; Dabrowiak, J. C. *Inorg. Chem.* **1975**, *14*, 296.
(15) Kimura, E.; Shionoya, M.; Yamauchi, T.; Shiro, M. *Chem. Lett.* **1991**, 1217.
(16) Chan, P. K.; Poon, C.-K. *J. Chem. Soc., Dalton Trans.* **1976**, 858.
(17) Daugherty, P. A.; Glerup, J.; Goodson, P. A.; Hodgson, D. J.; Michelsen, K. *Acta Chem. Scand.* **1991**, *45*, 244.
(18) Létumier, F.; Broeker, G.; Barbe, J.-M.; Guilard, R.; Lucas, D.; Dahaoui-Gindrey, V.; Lecomte, C.; Thouin, L.; Amatore, C. *J. Chem. Soc., Dalton Trans.* **1998**, 2233.
(19) Bucher, C. Ph.D. Thesis, Université de Bourgogne, Dijon, France, 1999.
(20) Bucher, C.; Duval, E.; Barbe, J.-M.; Verpeaux, J.-N.; Amatore, C.; Guilard, R. *C. R. Acad. Sci.* **2000**, *3*, 211.
(21) Jubran, N.; Cohen, H.; Koresh, Y. *J. Chem. Soc., Chem. Commun.* **1984**, 1683.
(22) Blake, A. J.; Gould, R. O.; Hyde, T. I.; Schröder, M. *J. Chem. Soc., Chem. Commun.* **1987**, 1730.
(23) Blake, A. J.; Gould, R. O.; Hyde, T. I.; Schröder, M. *J. Chem. Soc., Chem. Commun.* **1987**, 431.
(24) Golub, G.; Cohen, H.; Meyerstein, D. *J. Chem. Soc., Chem. Commun.* **1992**, 397.
(25) Golub, G.; Zilbermann, I.; Cohen, H.; Meyerstein, D. *Supramol. Chem.* **1996**, *6*, 275.
(26) Reimer, S.; Wicholas, M.; Scott, B.; Willet, R. D. *Acta Crystallogr., Sect. C* **1989**, 1694.
(27) Alcock, N. W.; Herron, N.; Moore, P. *J. Chem. Soc., Dalton Trans.* **1978**, 1282.
(28) Lincoln, S. F.; Coates, J. H.; Hadi, D. A. *Inorg. Chim. Acta* **1984**, *81*, L9.
(29) Wagner, F.; Mocella, M. T.; D'Aniello, M. J.; Wang, A. H. J.; Barefield, E. K. *J. Am. Chem. Soc.* **1974**, *96*, 2625.
(30) Moore, P.; Sachinidis, J.; Willey, G. R. *J. Chem. Soc., Chem. Commun.* **1983**, 522.
(31) Barefield, E. K.; Freeman, G. M.; Van Derveer, D. G. *Inorg. Chem.* **1986**, *25*, 552.
(32) Lee, T. J.; Lee, T. Y.; Hong, C. Y.; Wu, D. T.; Chung, C. S. *Acta Crystallogr., Sect. C* **1986**, 999.
(33) Hodges, K. D.; Wollmann, R. G.; Barefield, E. K.; Hendrickson, D. N. *Inorg. Chem.* **1977**, *16*, 2746.
(34) Hodges, K. D.; Wollmann, R. G.; Kessel, S. L.; Hendrickson, D. N.; Van Derveer, D. G.; Barefield, E. K. *J. Am. Chem. Soc.* **1979**, *101*, 906.

10.1021/ic001472h CCC: $20.00
Published on Web 09/27/2001

Experimental Section

Magnetic Studies. Magnetic studies were performed in the Laboratoire de Chimie Inorganique et Biologique du CEA-Grenoble on a Quantum Design MPMS SQUID magnetometer at temperatures from 2 to 300 K at two magnetic fields of 0.5 and 2.5 T. The sample (ca. 41 mg) was introduced in a kel F bucket whose contribution was measured independently and subtracted from the sample data. The diamagnetic contribution of the sample was estimated to be ca. -480×10^{-6} cm^3/mol using Pascal's constants.

EPR Spectroscopy. EPR spectra were recorded in the Laboratoire de Chimie Inorganique et Biologique du CEA-Grenoble on a Bruker EMX spectrometer equipped with an Oxford Instrument ESR 900 cryostat. The Bruker Microwave Bridge ER 041 XG is associated with a Bruker ER 4116 DM cavity. Powder spectra were obtained with ca. 0.7(5) mg of complex.

Electrochemistry. All electrochemical experiments were run under argon in the Département de Chimie de l'Ecole Normale Supérieure de Paris. *n*-Bu_4NBF_4 was used as the supporting electrolyte; it was obtained from *n*-$Bu_4N(HSO_4)$ and $NaBF_4$, recrystallized from ethyl acetate/hexane and dried at 60 °C under vacuum.

Cyclic voltammetry experiments were performed in an airtight three-electrode cell connected to a vacuum line. A SCE (Tacussel) reference electrode was separated from the solution by a bridge compartment filled with the same supporting electrode solution as that used in the cell. The counter electrode was a platinum spiral wire with ca. 1 cm^2 of apparent surface area. The working electrodes were disks obtained from cross sections of gold wires (diameter from 25 to 500 μm). An EG&G PAR-175 signal generator was used; the potentiostat was homemade and had a positive feedback loop for ohmic drop condensation. The current and potential were recorded on a Nicolet 310 oscilloscope.

Chronoamperometry Experiments and Determination of ρ. In the first series of experiments, the potential was set between the two oxidation waves (ca. 1.30 V) and the diffusional current i_1 for the first oxidation was measured as a function of the duration of the step (the precise and best value of the step potential was determined from the stationarylike graph built from the plot of the diffusional current as a function of the potential for a given value of the step duration). In a second series of experiments, the step potential was set after the second oxidation wave (ca. 1.5 V) and the total current i_{1+2} was measured. ρ was then calculated as $\rho = i_2/i_1 = (i_{1+2} - i_1)/i_1$.

Mass Spectrometry. Mass spectra were recorded in the Laboratoire d'Ingénierie Moléculaire pour la Séparation et les Applications des gaz de l'Université de Bourgogne on a Kratos Concept 32S by liquid secondary ion mass spectrometry (LSIMS, *m*-nitrobenzyl alcohol as the matrix).

Crystallographic Data Collection and Refinement of the Structure. Crystals of [(tmc)MnCl]BPh_4·CH_3CN are colorless. The diffraction intensities of a 0.40 × 0.34 × 0.24 mm crystal were collected with graphite-monochromatized Mo Kα X-radiation using an Enraf-Nonius CAD4F diffractometer at room temperature and the $\omega-2\theta$ scan technique to a $2\theta_{max}$ value of 50.0°. A total of 6205 reflections were measured, of which 5008 were considered to be significant, with $I_{net} > 2.0\sigma(I_{net})$, and used in the structure determination. The intensities of three standard reflections, measured every 200 reflections, remained constant throughout the data collection. Data reductions, including Lorentz polarization corrections, were carried out using the DREAR package.[35] No absorption correction was applied.

The structure was solved by Patterson methods and successive Fourier synthesis and then refined by full-matrix least squares.[36] After the location of all non-H atoms of the macrocyclic ligand and of the BPh_4 group, difference electron density maps showed four residual peaks: two of these are carbon atoms of the CH_3CN molecule (C39 and C40), whereas the two others are attributed to a disordered nitrogen atom. All these atoms were taken into account in the refinement. The occupancy factor of both disordered nitrogen atoms was fixed to 0.50.

Table 1. Summary of Crystallographic Data for [(tmc)MnCl]BPh_4·CH_3CN (**1**)

empirical formula	$C_{40}H_{55}BClMnN_5$
fw	707.09
system	triclinic
space group	*P*-1
a, *b*, *c* (Å)	11.514(2), 13.300(3), 14.225(3)
α, *β*, *γ* (deg)	74.86(3), 72.61(3), 74.31(3)
V (Å^3), *Z*	1962.4(7), 2
D_x (g/cm^3)	1.197
μ (mm^{-1})	0.438
T (K)	293
graphite-monochromated radiation	Mo Kα ($\lambda = 0.7107$ Å)
R1, wR2[a]	0.0594, 0.1630

[a] $R1 = \sum[k^{-1}|F_o| - |F_c|]/\sum|F_o|$, $wR2 = (\sum w[k^{-1}|F_o| - |F_c|]^2/\sum w|F_o|^2)^{1/2}$.

The scattering factors were taken from ref 37. All atoms except hydrogens were refined anisotropically. H-atoms were refined riding on their parent atoms with isotropic displacement parameters fixed at 1.2 or 1.5 (for methyl H-atoms) times the U_{eq} of the parent atoms. Statistics of the least-squares fit are given in Table 1.

Final fractional coordinates and equivalent isotropic thermal parameters of non-H atoms, positional parameters for H-atoms, a table of anisotropic thermal motion parameters, bond distances, and valence and torsion angles not included in Table 1 can be viewed in Supporting Information. Data for this structure have been deposited with the Cambridge Crystallographic Data Centre as supplementary publication no. CCDC-170554.

Chemicals. Solvents of reagent grade were purified and dried by conventional procedures prior to use. $MnCl_2$·xH_2O, tetrabutylamonium tetrafluoroborate, and sodium tetraphenylborate were dried by heating for several days under vacuum. The synthesis of 1,4,8,11-tetramethyl-1,4,8,11-tetraazacyclotetradecane (tmc) has been performed using a previously described procedure.[38]

[(tmc)MnCl]BPh_4·CH_3CN. Under argon, a solution of anhydrous $MnCl_2$ (0.26 g, 2 mmol) in methanol (20 mL) was added to a solution of freshly distilled tmc (0.50 g, 1.95 mmol) in the same solvent (20 mL). The resultant colorless mixture was stirred for 2 h at room temperature, and 1.7 g (4.9 mmol) of anhydrous sodium tetraphenylborate was added. After the mixture was stirred for 30 min, the white precipitate was collected, washed several times with methanol, and recrystallized from acetonitrile. The slow cooling of the solution to room temperature yielded colorless crystals of [(tmc)MnCl]BPh_4·CH_3CN (0.99 g, 70%). MS (LSIMS) *m*/*z*: 346.2 ([(tmc)MnCl]$^+$). Anal. Calcd (found) for $C_{40}N_5H_{55}BMnCl$: C, 67.95 (67.88); H, 7.85 (7.83); N, 9.91 (9.85).

[(tmc)MnCl]BF_4. Under argon, a solution of anhydrous $MnCl_2$ (0.54 g, 4.2 mmol) in acetonitrile (20 mL) was added to a solution of freshly distilled tmc (1.1 g, 4.3 mmol) in the same solvent. The resultant mixture was stirred for 2 h at room temperature, and 1.5 g (4.7 mmol) of TBA(BF_4) was added. Acetonitrile was then removed under reduced pressure until a white solid precipitated. After filtration, slow evaporation of the colorless solution yielded a pale green crystal of [(tmc)MnCl]BF_4 (1.4 g, 75%). MS (LSIMS) *m*/*z*: 346.2 ([(tmc)MnCl]$^+$). Anal. Calcd (found) for $C_{14}N_4H_{32}BMnClF_4$: C, 38.78 (38.56); H, 7.44 (7.39); N, 12.92 (12.67).

Results and Discussion

Molecular Structure of [(tmc)MnCl]BPh_4·CH_3CN. The structure of the cation in [(tmc)MnCl]BPh_4·CH_3CN is shown in Figure 1, and main bond distances and angles are listed in Table 2. The Mn ion lies in a distorted square-pyramidal coordination involving the four N atoms of the macrocyclic

(35) Blessing, R. H. *Crystallogr. Rev.* **1987**, *1*, 3.
(36) Sheldrick, G. M. *SHELX76: Program for Crystal Structure Determination*; University of Göttingen: Göttingen, Germany, 1976.
(37) Cromer, D. T.; Waber, J. T. *International Tables for X-ray Crystallography*; The Kynoch Press: Birmingham, 1974; Vol. 4.
(38) Royal, G.; Dahaoui-Gindrey, V.; Dahaoui, S.; Tabard, A.; Guilard, R.; Pullumbi, P.; Lecomte, C. *Eur. J. Org. Chem.* **1998**, *1*, 1971.

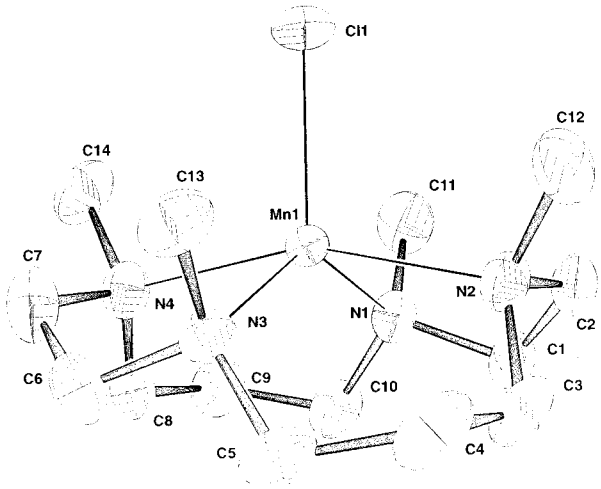

Figure 1. ORTEP view of $[(tmc)MnCl]^+$ in $[(tmc)MnCl]BPh_4 \cdot CH_3CN$ (hydrogen atoms are omitted for clarity). Ellipsoids are drawn at a 50% probability level.

Table 2. Interatomic Distances (Å) and Angles (deg) Relevant to the Manganese Coordination Spheres in **1**

bond	value (Å)	bond	value (Å)
Mn−N3	2.228(3)	Mn−N4	2.281(3)
Mn−N2	2.256(3)	Mn−Cl1	2.331(1)
Mn−N1	2.258(3)		
angle	**value (deg)**	**angle**	**value (deg)**
N3−Mn−N2	90.6(2)	N1−Mn−N4	89.9(2)
N3−Mn−N1	135.0(2)	N3−Mn−Cl1	114.4(1)
N2−Mn−N1	81.5(2)	N2−Mn−Cl1	101.2(1)
N3−Mn−N4	81.2(2)	N1−Mn−Cl1	110.6(1)
N2−Mn−N4	158.1(2)	N4−Mn−Cl1	100.7(1)

ligand in the basal plane and one Cl ion in the apical position. The Mn atom is displaced 0.645 Å out of the N1, N2, N3, N4 least squares toward the apical chlorine and on the same side as *N*-methyl groups. The Mn−Cl distance (2.331(2) Å) is very short compared to those found in the pseudo-octahedral manganese(III) complexes such as $[(cyclam)Mn(III)Cl_3]$ and $[(cyclam)Mn(III)Cl_2NO_3]$ of 2.5269(7) and 2.526(1) Å, respectively.[17,39] The large Mn(II)−N distances (2.23−2.28 Å) are in agreement with a high-spin Mn ion in a +II oxidation state, as shown by comparison with Mn(III)−N distances ($\langle Mn(III)-N \rangle = 2.03$ Å).[17,39] The four *N*-methyl groups of the macrocyclic ligand are located on the same side of the cation, giving the *trans*-(*R*,*S*,*R*,*S*)-I form (R═CH_3) according to Bosnich et al.[40]

Magnetization. Magnetic measurements were performed at two fields at temperatures from 2 to 300 K. Between 30 and 300 K, the Mn displayed essentially a Curie behavior. The fit of the magnetization vs $\beta H/kT$ by a Brillouin's function with $S = 5/2$ fixed gave $g = 2.04$. It was not necessary to add any other parameters as a paramagnetic impurity or temperature-independent paramagnetism (TIP). These measurements are thus in accordance with a mononuclear high-spin Mn(II) species.

EPR. The EPR spectrum of the manganese complex is depicted in Figure 2. It is visible at temperatures from 4.2 K to room temperature, although some line broadening appears above 170 K. While temperature variation has little effect on the main features, some variations of the spectrum are observed especially at high field.

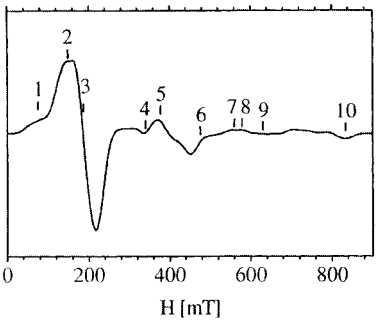

Figure 2. EPR spectrum of $[(tmc)MnCl]BPh_4 \cdot CH_3CN$ recorded at 4 K (the assignment of the EPR transitions is given in Table 3).

The spectrum does not present hyperfine transitions. Moreover, considerable overlapping of transitions makes it very complicated, and a detailed interpretation is difficult. Similar EPR spectra are obtained for the powder and diluted acetonitrile frozen solutions. Therefore, the large line width is not due to spin−spin intermolecular interactions. The EPR spectrum of this compound is very different from previously reported ones, with a small line at $g = 11$, the main derivative line at $g = 3.7$, some lines close to $g = 1.8$, and transitions at more than 900 mT.

In 1968, Dowsing and Gibson calculated the EPR line positions for a d^5 system for a range of *D* and *E* values.[41] In 1970, Aasa added the line position off-axis transitions observable in powder or frozen solution spectra.[42] In 1992, Mabbs and Collison gave several simulations of d^5 compounds.[43] These are essential to interpret correctly the experimental spectra, as their shape cannot be estimated easily and precisely from a diagram representing the transition positions. *D* and *E* values were first estimated by determining the range of values furnishing acceptable concordances with simulated spectra of Mabb and Collison (see ref 43, pp 904−942). This led to estimated *D* values in the range of 0.2−0.4 cm^{-1} and close to 0.25 cm^{-1} and *E*/*D* values in the range of 0.17−0.25 and close to 0.25 cm^{-1}. All the major spectral features are reproduced in the spectrum calculated for $D = 0.2$ cm^{-1} and $E/D = 0.27$ (see ref 43, Figure 14.66e, p 921). Moreover, values of $D = 0.24$ cm^{-1} and $E/D = 0.25$ give good correspondence between the spectrum and the expected positions of the transitions from the frequency-independent resonance (FIR) diagram (see ref 43, Figure 14.93a). These lines are consistent with the position determined in the more complete diagram of Aasa (see ref 42, Figures 1, 2, and 7 at $E/D = 0.25$). For more transitions, extra powder lines are often found when the field lies in any of the principal planes but not along the axes. Some of these off-axis lines are included in the latter diagram. They explain, for example, the last bump at high field and also some transitions close to $g = 1.8$. The transition assignments are reported in Table 3.

Generally, Mn(II) EPR spectra are highly resolved with relatively narrow line widths, which allow the observation of ^{55}Mn hyperfine coupling. However, broad resonances in solid and frozen solution EPR spectra have been reported for low-symmetry mononuclear Mn(II) complexes.[44] Nevertheless, EPR fine-splitting patterns may arise not only from monomeric species but also from species with higher nuclearity. For example, fine structure is well documented for 2Mn(II,II) pairs.[45]

(39) Dahaoui-Gindrey, V. Ph.D. Thesis, Université Henri Poincaré, Nancy I, 1995.
(40) Bosnich, B.; Poon, C. K.; Tobe, M. L. *Inorg. Chem.* **1965**, *4*, 1102.
(41) Dowsing, R. D.; Gibson, J. F. *J. Chem. Phys.* **1969**, *50*, 294.
(42) Aasa, R. J. *J. Chem. Phys.* **1970**, *52*, 3919.
(43) Mabbs, F. E.; Collison, D. *Electron Paramagnetic Resonance of Transition Metal Compounds*; Elsevier: Amsterdam, 1992; Vol. 16.
(44) Dowsing, R. D.; Gibson, J. F.; Goodgame, M.; Hayward, P. J. *J. Chem. Soc. A* **1969**, 187.

Table 3. Assignment of EPR Transitions

line number	field (mT)	transition[a]
1	75	y (1 → 2), z (5 → 6)
2	150	z (3 → 4)
3	185	x (3 → 4)
4	338	z (3 → 4)
5	372	x (1 → 2)
6	488	yz (3 → 4)
7	561	x (5 → 6)
8	575	y (3 → 4)
9	620	z (3 → 4)
10	834	yz (3 → 4)

[a] See ref 42.

In the absence of hyperfine structure, the occurrence of Mn pairs of larger clusters may thus be difficult to exclude, but magnetization measurements ruled out the latter possibility. Therefore, the fine structure in the EPR spectrum is due to a distorted mononuclear species rather than to the presence of Mn clusters.

The literature mentions only a few pentacoordinated Mn(II) complexes whose X-ray structures and EPR characterizations are available. To the best of our knowledge, this compound is the first non-porphyrinic square-pyramidal complex with both structural and EPR characterizations. Three limiting cases are usually found: the main lines are located either close to $g = 2$ for a cubic symmetry, close to $g = 6$ and $g = 2$ for an axial symmetry ($E = 0$), or close to $g = 4.3$ for a fully rhombic symmetry (E/D is close to 1/3). This compound has a strikingly different EPR spectrum with the main derivative line at $g =$ 3.7 and transitions at more than 900 mT. This peculiarity is associated with D and E/D values close to 0.25 cm^{-1} and 0.25, respectively. The large D and E values reflect the axial distortion of the tetragonal symmetry and the rhombic distortion within the equatorial plane, respectively. Indeed, the geometry of the manganese ion appears to be intermediate between a distorted square pyramid with an apical chloride and a trigonal bipyramid with an N2N4 axis.

Electrochemistry. In agreement with the general trend of *N*-tetrasubstituted cyclam derivatives stabilizing low oxidation states, the oxidation of [(tmc)MnCl]BF_4 was found to require high potential values. The standard potential was measured at $E° = 1.14$ V vs SCE in acetonitrile.

At potential scan rates higher than 10 V/s, the cyclic voltammogram recorded in acetonitrile exhibits only one monoelectronic oxidation wave, which appears to be fully chemically reversible. The peak to peak separation ΔE^p varies from 75 to 140 mV when the potential scan rate increases from 0.1 to 100 V/s, even with ohmic drop compensation; this is indicative of a slow heterogeneous electron transfer. Voltammograms recorded at 2 V/s or less show a second reversible oxidation wave ($E° = 1.36$ V), the size of which increases with decreasing potential scan rate (Figure 3A,B). This observation supports the transformation, on the time scale of slow cyclic voltammetry, of the initially formed $[(tmc)MnCl]^{2+}$ into another species.

In our experimental conditions, the oxidation of authentic Cl^- takes place at 1.30 V (peak potential), leading to a broad, chemically irreversible wave. Although it happens in the same potential range, the rather ill-defined wave is clearly different from the reversible couple observed ($E° = 1.36$ V associated with an oxidation peak potential E^p at 1.40 V) upon the oxidation of our manganese derivative. Accordingly, it establishes that Cl^- is not released during the first electrochemical process.

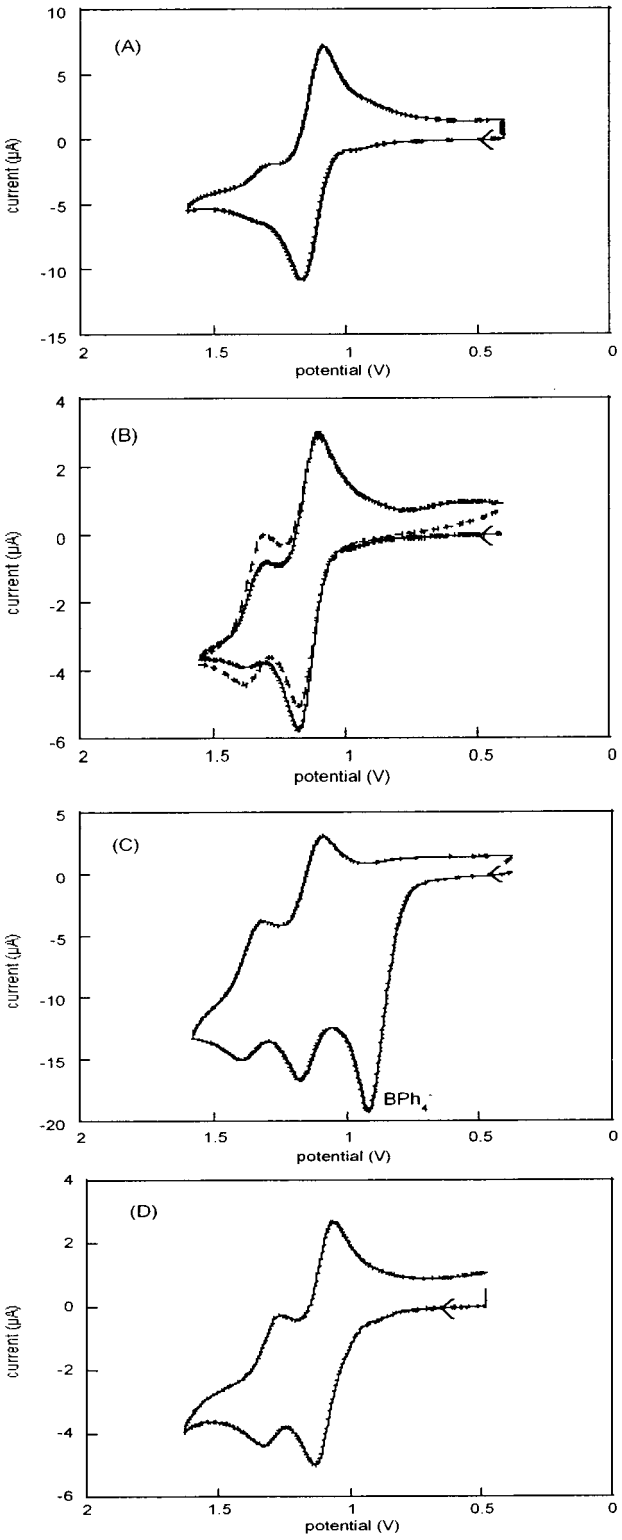

Figure 3. Cyclic voltammograms of approximately 2 mM solutions of $[(tmc)MnCl]^+ \cdot X^-$ in acetonitrile and 0.1 M Bu_4NBF_4 at a platinum electrode and room temperature: (A) X = BF_4, 2 V/s; (B) X = BF_4, 0.5 V/s, first scan is shown in full line, second scan in dotted line; (C) X = BPh_4, 2 V/s; (D) X = BF_4, 2 V/s where 1.6 mM (0.8 molar equiv) HBF_4 was added.

The new electroactive product has to be another chloromanganese derivative; the electron stoichiometry observed favors a manganese(III) species, and the decoordination of the tmc ligand

(45) Gelasco, A.; Kirk, M. L.; Kampf, J. W.; Pecoraro, V. L. *Inorg. Chem.* **1997**, *36*, 1829.

Scheme 1

$$[(tmc)MnCl]^{+}, BF_4^{-} \; -e \rightleftharpoons [(tmc)MnCl]^{2+}, BF_4^{-} \qquad E^0 = 1.14\ V$$

$$[(tmc)MnCl]^{2+}, BF_4^{-} \longrightarrow \text{Mn(III) complex} \qquad \textit{reaction I}$$

$$\text{Mn(III) complex} \; -e \rightleftharpoons \text{Mn(IV) complex} \qquad E^0 = 1.36\ V$$

appears very unlikely. Therefore, reaction I in Scheme 1 is best described as an isomerization process.[46]

As expected, the second wave appears more prominently on the second scan than on the first (Figure 3B). Digital simulation[47] of the experimental voltammograms based on the mechanism above provided a very good fit for both the first and second oxidation waves and allowed the determination of the rate constant for the isomerization process as $k = 0.3\ s^{-1}$.

When the tetrafluoroborate counteranion was replaced by tetraphenylborate (Figure 3C), the size of the oxidation wave at 1.36 V clearly increased. This showed that, in a given time corresponding to a given potential scan rate, the conversion of $[(tmc)MnCl]^{2+}$ into a Mn(III) complex in reaction I (Scheme 1) had occurred to a greater extent. Note that in this latter case, the two oxidation waves associated with the manganese cation are preceded by an irreversible bielectronic wave, which could easily be assigned to the oxidation of BPh_4^-. This surprising result was tentatively interpreted with an acidic catalysis for the isomerization process between $[(tmc)MnCl]^{2+}$ and the Mn(III) complex. Indeed, in aprotic medium, the two-electron oxidation of BPh_4^- is known to generate a strong Lewis acid[48−50] in the diffusion layer when and where the oxidation of $[(tmc)MnCl]^+$ takes place. This hypothesis could be confirmed by a series of voltammetric experiments run in the presence of increasing amounts of *p*-toluenesulfonic or tetrafluoroboric acid. Figure 3D illustrates the role of acids in the isomerization process. Chronoamperometry measurements at various potential step durations allowed us to determine the ratio $\rho = i_2/i_1$ of the diffusional currents associated with the second and first oxidation waves. In the absence of added acid, ρ varies from 2% at 20 ms to 25% at 300 ms. In the presence of approximately 0.5 equiv of HBF_4 etherate complex, ρ is equal to 27% at 20 ms and reaches 68% at 300 ms.[46]

The structure of the Mn(III) product formed from $[(tmc)MnCl]^{2+}$ could not be elucidated on the basis of voltammetric data. The efficiency of acids as catalysts for this isomerization may suggest a modification of the configuration of the ligand with an inversion of some nitrogen centers. The new Mn(III) product can be oxidized within the potential window ($E° = 1.36$ V), whereas the initially formed pentacoordinated manganese(III) complex, deriving from the starting Mn(II) by electron uptake, cannot (single oxidation wave at a high-potential scan rate, when the isomerization process is kinetically frozen). This fact supports an increase in the coordination number and, finally, makes an isomerization from configuration I to hexacoordinated *trans*-III a rather likely hypothesis.

Supporting Information Available: Listing of crystal data and structure refinement, atomic coordinates ($\times 10^4$) and equivalent isotropic displacement parameters ($\times 10^3$ Å^2), bond lengths (Å) and angles (deg), and anisotropic displacement parameters ($\times 10^3$ Å^2) for $[(tmc)MnCl]$-BPh_4·CH_3CN. This material is available free of charge via the Internet at http://pubs.acs.org.

IC001472H

(46) $[(tmc)MnCl]^{2+}$, initially formed from $[(tmc)MnCl]^+$ at the monoelectronic first oxidation wave, undergoes a follow-up chemical reaction, the product of which is oxidized at the second oxidation wave. Since this reaction involves no other electron transfer and no decoordination step, two possibilities should be considered: either a change of configuration (isomerization) of the mononuclear manganese(III) or a dimerization. The possible involvement of a dimer has been examined since the size of the second oxidation wave (smaller and reaching roughly one-half of the size of the first wave when the follow-up reaction proceeds efficiently, either with the BPh_4^- anion or acidic catalysis) seemed to fit with the 1:2 current ratio expected for a monoelectronic oxidation of a dimer formed from the monoelectronic oxidation of the monomer precursor. However, in acidic media, the size of the second oxidation wave can overtake 50% of the size of the first one and can even come very close to 100% of the first wave size when more than 1 molar equiv of acid is added; unfortunately, under these conditions, a substantial loss of material occurs (as seen by the decrease in the size of the first oxidation wave). Simultaneously, the solution turned cloudy, in agreement with an acid-promoted decoordination of the macrocyclic ligand. More definitive evidence against a dimerization process was given by the absence of any concentration effect: no significant change of the relative size of the two waves could be perceived when the concentration of $[(tmc)MnCl]^+$, BPh_4^- was increased from 0.6×10^{-3} to 4×10^{-3} M.

(47) The simulations were performed using the program *Digisim 2.1* Rudolph, M.; Feldberg, S. W. Bioanalytical Systems, Inc.

(48) Geske, D. *J. Phys. Chem.* **1959**, *63*, 1062.
(49) Horii, H.; Taniguchi, S. *J. Chem. Soc., Chem. Commun.* **1986**, 915.
(50) Bancroft, E.; Blount, H.; Janzen, E. *J. Am. Chem. Soc.* **1979**, *101*, 3692.